J. Phys. Res. Edu., Vol. 2, March 2025

Thermodynamic properties of the α-T_3 quantum ring

Mijanur Islam[1,2*]

[1]*Department of Physics, Indian Institute of Technology-Guwahati, Guwahati-781039, India.*

[2]*Department of Physics, University of Ottawa, Ottawa, K1N6N5, Canada.*

Here, we investigate the thermodynamic properties of an α-T_3 quantum ring (QR) in presence of an external perpendicular magnetic field. We use coordinate transformation to describe the energy spectra of the quantum ring. In addition, we delve into the thermodynamic properties of the QR when it is exposed to a uniform magnetic field within a heat bath. To facilitate this, we employ the partition function obtained through the Euler-Maclaurin formula. In particular, we analyze the energy spectrum and the behaviour of fundamental thermodynamic functions in the canonical ensemble. These include the Helmholtz free energy, internal energy, entropy, and heat capacity. Notably, our study verifies the adherence to the Dulong-Petit law in both cases.

I. INTRODUCTION

From the past few decades quantum rings (QRs) have attracted considerable interest owing to their wide range of practical applications, which include the uses of QRs as single photon emitters, nanoflash memory devices [1, 2], detectors of photons [3], further as the qubits in quantum computing, [1] etc.

The α-T_3 lattice has attracted substantial interest due to its tunable electronic properties. By varying the parameter α in the range from 0 to 1, this system provides an uniform interpolation among the honeycomb lattice of graphene with $\alpha = 0$ and the dice lattice with $\alpha = 1$ [4–6]. Observational realizations of an α-T_3 lattice have been proposed in engineered heterostructures and optical lattice configurations [7–9]. The nearest-neighbor tight-binding investigation reveals that these systems host massless Dirac-Weyl quasiparticles, with a generalized pseudospin structure that depends continuously on the parameter α. In recent years, extensive research has been devoted to investigating the rich topological and transport properties of the α-T_3 lattice, encompassing phenomena such as magneto-optical effects, RKKY interactions, minimal conductivity, spin Hall responses, and topological phase transitions [12–18].

Motivated by the emerging potential of QRs, in this study we investigate the influence of a central magnetic flux on an α-T_3 quantum ring. From a theoretical standpoint, it is crucial to develop a comprehensive understanding of how the interplay between the tunable parameter α, the applied magnetic field, and quantum confinement in reduced dimensions collectively governs charge transport. These intertwined effects have a direct bearing on the system's electronic behaviour and significantly influence its thermodynamic

properties. Moreover, the exploration of the physical properties of such materials, with a particular focus on their thermal characteristics, holds significant importance in condensed matter physics, particularly in the context of solid-state materials. This endeavor is driven by both practical requirements and the pursuit of fundamental scientific knowledge [19]. It is noteworthy that previous works [20–23] have explored the thermoelectric properties of materials like graphene, carbon nanotubes, graphite, nanostructure carbon materials etc. This study aims to shed light on the thermodynamic properties of an α-T_3 quantum ring. To achieve these, we consider a set of non-interacting and indistinguishable N-fermions which are confined within a QR. The observation enables us to adopt an approach which works well in the strong field limit and utilize a numerical method which is based on the much celebrated Euler-Maclaurin formula to compute the canonical partition function. Notably, our results demonstrate the recovery of the famous Dulong-Petit law as a limiting case.

The paper is organized as follows. In Section , we present the model. Section and Sec. provide the explicit formulas and discussion of thermodynamic properties, respectively. Finally, our findings are summarized in Section .

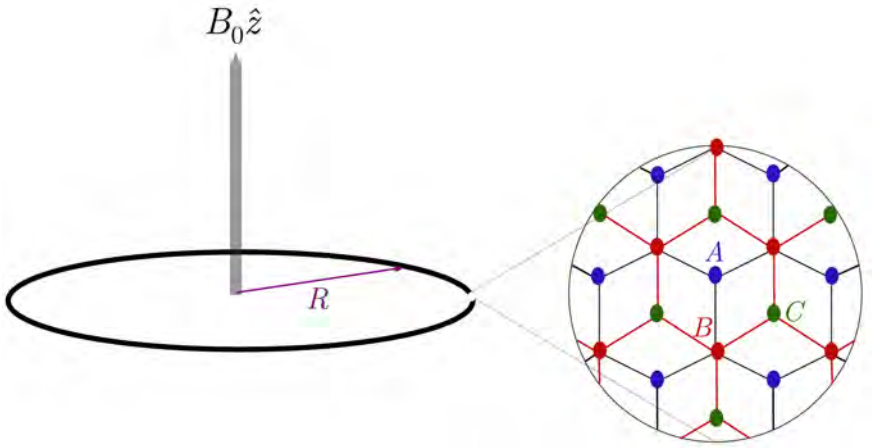

FIG. 1. A schematic diagram of an α-T_3 QR of radius R subjected to a perpendicular magnetic field $\mathbf{B} = B_0\hat{z}$ is shown. The zoomed-in section illustrates the α-T_3 lattice structure, where the inequivalent lattice sites A, B, and C are represented by blue, red, and green dots, respectively.

II. α-T_3 QUANTUM RING

We consider a QR having radius R lying in the cartesian x-y plane, composed of an α-T_3 lattice, as illustrated in Fig.1. A magnified view highlights the underlying structure of the lattice. An α-T_3 unit cell consists of three inequivalent lattice sites, namely, A, B, and C sites. The lattice sites A and B construct

a honeycomb structure, identical to that of graphene, and are connected via a nearest-neighbor hopping strength t. In contrast, the central C site is connected exclusively to the three surrounding B sites by a reduced hopping amplitude αt, where $0 < \alpha \leq 1$. This tunable parameter α enables a continuous crossover from graphene ($\alpha = 0$) to the dice lattice ($\alpha = 1$). The QR is subjected to a magnetic field $\boldsymbol{B} = B_0\hat{z}$ which is perpendicular to the plane. In the vicinity of a particular valley (K or K′) the low energy excitations of the α-T_3 lattice can be expressed via the Dirac-Weyl Hamiltonian,

$$H^{\xi} = v_F \mathbf{S} \cdot \boldsymbol{\pi}, \tag{1}$$

where v_F denotes the Fermi velocity, $\xi = \pm 1$ is the valley index, and π_x and π_y are the components of the canonical momentum operator defined as $\boldsymbol{\pi} = \boldsymbol{k} + e\boldsymbol{A}$, where $\boldsymbol{k}$ and $\boldsymbol{A}$ denote the in-plane momentum operator and the magnetic vector potential respectively. Further, x and y components of the pseudospin operator $\boldsymbol{S}$ associated with the α-T_3 lattice are defined via,

$$S_x = \xi \begin{pmatrix} 0 & \cos\varphi & 0 \\ \cos\varphi & 0 & \sin\varphi \\ 0 & \sin\varphi & 0 \end{pmatrix} \quad \text{and} \quad S_y = -i \begin{pmatrix} 0 & \cos\varphi & 0 \\ -\cos\varphi & 0 & \sin\varphi \\ 0 & -\sin\varphi & 0 \end{pmatrix}, \tag{2}$$

respectively, with $\tan\varphi = \alpha$, implying that a tunability for graphene to dice lies in the parameter φ.

Since $\boldsymbol{B} = B_0\hat{z}$, we choose $\boldsymbol{A}$ in the symmetric gauge as $\boldsymbol{A} = B_0(-y\hat{x} + x\hat{y})$. For circular symmetry of the system it is more suitable to write $\boldsymbol{A}$ in the polar coordinates (r, θ) as $\boldsymbol{A} = \frac{1}{2} r B_0 \hat{\theta}$.

Therefore, we can write the Hamiltonian of Eq. (1) using Eq. (2) as,

$$H^{\xi} = v_F \begin{pmatrix} 0 & \{\xi(k_x + eA_x) - i(k_y + eA_y)\}\cos\varphi & 0 \\ \{\xi(k_x + eA_x) + i(k_y + eA_y)\}\cos\varphi & 0 & \{\xi(k_x + eA_x) - i(k_y + eA_y)\}\sin\varphi \\ 0 & \{\xi(k_x + eA_x) + i(k_y + eA_y)\}\sin\varphi & 0 \end{pmatrix}. \tag{3}$$

Now we transform $v_F(k_x + eA_x - ik_y - ieA_y)$ into the polar coordinates (r, θ) using the transformations as follows,

$$\begin{aligned} & v_F(k_x + eA_x - ik_y - ieA_y) \\ &= v_F\bigg(-i\hbar\frac{\partial}{\partial x} - \frac{eB_0 y}{2} + i^2\hbar\frac{\partial}{\partial y} - i\frac{eB_0 x}{2}\bigg) \\ &= v_F\bigg[-i\hbar\big(\cos\theta\frac{\partial}{\partial r} - \frac{\sin\theta}{r}\frac{\partial}{\partial\theta}\big) - \frac{eB_0 r\sin\theta}{2} - \hbar\big(\sin\theta\frac{\partial}{\partial r} + \frac{\cos\theta}{r}\frac{\partial}{\partial\theta}\big) - i\frac{eB_0 r\cos\theta}{2}\bigg] \\ &= \hbar v_F\bigg[-i\big(\cos\theta - i\sin\theta\big)\frac{\partial}{\partial r} - \big(\cos\theta - i\sin\theta\big)\frac{1}{r}\frac{\partial}{\partial\theta} - \frac{ieB_0 r}{2\hbar}\big(\cos\theta - i\sin\theta\big)\bigg] \\ &= \hbar v_F\, e^{-i\theta}\bigg[-i\frac{\partial}{\partial r} - \frac{1}{r}\frac{\partial}{\partial\theta} - \frac{ieB_0 r}{2\hbar}\bigg]. \end{aligned} \tag{4}$$

To derive the third line from the second line of the above equation, we use $x = r\cos\theta$, $y = r\sin\theta$, $\frac{\partial}{\partial x} = \cos\theta\frac{\partial}{\partial r} - \frac{\sin\theta}{r}\frac{\partial}{\partial\theta}$, and $\frac{\partial}{\partial y} = \sin\theta\frac{\partial}{\partial r} + \frac{\cos\theta}{r}\frac{\partial}{\partial\theta}$. Finally, $v_F(k_x + eA_x + ik_y + ieA_y)$ becomes $\hbar v_F\, e^{i\theta}(-i\frac{\partial}{\partial r} + \frac{1}{r}\frac{\partial}{\partial\theta} + \frac{ieBr}{2\hbar})$. The components of the vector potential are $A_r = 0$ and $A_\theta = \frac{Br}{2}$.

Therefore, the Hamiltonian in cylindrical coordinates becomes,

$$H^\xi = v_F(\mathbf{k} + e\mathbf{A})_{cyl} \cdot \mathbf{S}_{cyl}, \tag{5}$$

with $\mathbf{k} = (k_r, k_\theta)$, $\mathbf{A} = (A_r, A_\theta)$ and $S = (S_r, S_\theta)$, where $k_r = -i\hbar\frac{\partial}{\partial r}$, $k_\theta = -i\hbar\frac{1}{r}\frac{\partial}{\partial\theta}$, and the pseudospin components takes the form,

$$S_r = \begin{pmatrix} 0 & e^{-i\theta}\cos\varphi & 0 \\ e^{i\theta}\cos\varphi & 0 & e^{-i\theta}\sin\varphi \\ 0 & e^{i\theta}\sin\varphi & 0 \end{pmatrix}, \text{ and } S_\theta = \begin{pmatrix} 0 & -ie^{-i\theta}\cos\varphi & 0 \\ ie^{i\theta}\cos\varphi & 0 & -ie^{-i\theta}\sin\varphi \\ 0 & ie^{i\theta}\sin\varphi & 0 \end{pmatrix}. \tag{6}$$

After doing the transformations the final Hamiltonian at the two valleys (say K and K′) in the polar coordinates assumes a form,

$$H^\xi = \hbar v_F \begin{pmatrix} 0 & e^{-i\xi\theta}(-i\xi\frac{\partial}{\partial r} - \frac{1}{r}\frac{\partial}{\partial\theta} - \frac{ieB_0r}{2\hbar})\cos\varphi & 0 \\ e^{i\xi\theta}(-i\xi\frac{\partial}{\partial r} + \frac{1}{r}\frac{\partial}{\partial\theta} + \frac{ieB_0r}{2\hbar})\cos\varphi & 0 & e^{-i\xi\theta}(-i\xi\frac{\partial}{\partial r} - \frac{1}{r}\frac{\partial}{\partial\theta} - \frac{ieB_0r}{2\hbar})\sin\varphi \\ 0 & e^{i\xi\theta}(-i\xi\frac{\partial}{\partial r} + \frac{1}{r}\frac{\partial}{\partial\theta} + \frac{ieB_0r}{2\hbar})\sin\varphi & 0 \end{pmatrix}. \tag{7}$$

The Hamiltonian H^ξ in Eq. (1) commutes with the z-component of the total angular momentum operator denoted by $J_z = L_z + S_z$. Here $L_z(= -i\hbar\frac{\partial}{\partial\theta})$ and S_z represent the orbital angular momentum operator and the pseudospin contribution arising from the sublattice degrees of freedom in the α-T_3 lattice respectively. This makes it feasible to use the total angular momentum to be a good quantum number to characterize the energy levels. In polar coordinates, the eigenstates of Eq. (7) are given by,

$$\psi(r,\theta) = \begin{pmatrix} \chi_1(r)e^{iw\theta} \\ \chi_2(r)e^{im\theta} \\ \chi_3(r)e^{iq\theta} \end{pmatrix} \tag{8}$$

where w, m, and q are the angular momentum labels and χ_is denote the amplitudes corresponding to the three sublattices. Moreover, we consider a strictly one-dimensional (1D) ring of radius R such that the radial part is frozen in the eigensolution [24–26]. To ensure the Hermiticity of the Hamiltonian in the ring geometry, the following replacements should be made: $r \to R$ and $\frac{\partial}{\partial r} \to -\frac{1}{2R}$.

Further, solving $H^{\xi}\psi(r,\theta) = E\psi(r,\theta)$ at K valley ($\xi = 1$), we obtain,

$$\begin{aligned}
&\hbar v_F e^{-i\theta}\cos\varphi\Big(-i\frac{\partial}{\partial r} - \frac{1}{r}\frac{\partial}{\partial\theta} - \frac{ieB_0 r}{2\hbar}\Big)\chi_2(r)e^{im\theta} = E\chi_1(r)e^{iw\theta} \\
&\Rightarrow i\hbar v_F\cos\varphi\Big(\frac{1}{2R} - \frac{m}{R} - \frac{eB_0R}{2\hbar}\Big)\chi_2(R)e^{i(m-1)\theta} = E\chi_1(R)e^{iw\theta} \\
&\Rightarrow -E\chi_1(R) - i\frac{\hbar v_F}{R}\Big(m + \frac{\Phi}{\Phi_0} - \frac{1}{2}\Big)\chi_2(R)\cos\varphi = 0
\end{aligned} \tag{9}$$

with the condition $w = (m-1)$. Where $\Phi = \pi R^2 B_0$ being the magnetic flux threading the ring and $\Phi_0 = h/e$ the quantum of magnetic flux. Further,

$$\hbar v_F e^{i\theta}\cos\varphi\Big(-i\frac{\partial}{\partial r} + \frac{1}{r}\frac{\partial}{\partial\theta} + \frac{ieB_0 r}{2\hbar}\Big)\chi_1(r)e^{iw\theta} + \hbar v_F e^{-i\theta}\sin\varphi\Big(-i\frac{\partial}{\partial r} - \frac{1}{r}\frac{\partial}{\partial\theta} - \frac{ieB_0 r}{2\hbar}\Big)\chi_3(r)e^{iq\theta} = E\chi_2(r)e^{im\theta}$$

$$\Rightarrow i\hbar v_F\cos\varphi\Big(\frac{1}{2R} + \frac{w}{R} + \frac{eB_0R}{2\hbar}\Big)\chi_1(R)e^{i(w+1)\theta} + i\hbar v_F\sin\varphi\Big(\frac{1}{2R} - \frac{q}{R} - \frac{eB_0R}{2\hbar}\Big)\chi_3(R)e^{i(q-1)\theta} = E\chi_2(R)e^{im\theta}$$

$$\Rightarrow i\frac{\hbar v_F}{R}\Big(m + \frac{\Phi}{\Phi_0} - \frac{1}{2}\Big)\chi_1(R)\cos\varphi - E\chi_2(R) - i\frac{\hbar v_F}{R}\Big(m + \frac{\Phi}{\Phi_0} + \frac{1}{2}\Big)\chi_3(R)\sin\varphi = 0 \tag{10}$$

with the condition $w = m-1$ and $q = m+1$. Finally one gets,

$$\begin{aligned}
&\hbar v_F e^{i\theta}\sin\varphi\Big(-i\frac{\partial}{\partial r} + \frac{1}{r}\frac{\partial}{\partial\theta} + \frac{ieB_0 r}{2\hbar}\Big)\chi_2(r)e^{im\theta} = E\chi_3(r)e^{iq\theta} \\
&\Rightarrow i\hbar v_F\sin\varphi\Big(\frac{1}{2R} + \frac{m}{R} + \frac{eB_0R}{2\hbar}\Big)\chi_2(R)e^{i(m+1)\theta} = E\chi_3(R)e^{in\theta} \\
&\Rightarrow i\frac{\hbar v_F}{R}\Big(m + \frac{\Phi}{\Phi_0} + \frac{1}{2}\Big)\chi_2(R)\sin\varphi - E\chi_3(R) = 0
\end{aligned} \tag{11}$$

with the condition $q = m+1$. Similarly, at the other valley K′ ($\xi = -1$) the conditions are $w = m+1$ and $q = m-1$. Combining them, we obtain the following conditions that should be valid, namely,

$$w = m - \xi \;\text{ and }\; q = m + \xi. \tag{12}$$

Thus, the eigenstates corresponding to H^{ξ} can be derived as,

$$\psi^{m\xi}(R,\theta) = \begin{pmatrix} \chi_1(R)e^{i(m-\xi)\theta} \\ \chi_2(R)e^{im\theta} \\ \chi_3(R)e^{i(m+\xi)\theta} \end{pmatrix}, \tag{13}$$

where the integer m is the only independent total angular momentum quantum number (w and q depends on m through Eq. (12)). Therefore, the Hamiltonian corresponding to an ideal α-T_3 ring is given by,

$$H^{\xi}_{\text{ring}} = \frac{\hbar v_F}{R}\begin{pmatrix} 0 & -i\Big(m + \frac{\Phi}{\Phi_0} - \frac{\xi}{2}\Big)\cos\varphi & 0 \\ i\Big(m + \frac{\Phi}{\Phi_0} - \frac{\xi}{2}\Big)\cos\varphi & 0 & -i\Big(m + \frac{\Phi}{\Phi_0} + \frac{\xi}{2}\Big)\sin\varphi \\ 0 & i\Big(m + \frac{\Phi}{\Phi_0} + \frac{\xi}{2}\Big)\sin\varphi & 0 \end{pmatrix}. \tag{14}$$

We obtain the energy spectrum as,

$$E_1 = 0 \quad\text{and}\quad E_2^{\pm} = \pm\epsilon\sqrt{\Big(m + \frac{\Phi}{\Phi_0}\Big)^2 + \frac{1}{4} - \xi\Big(m + \frac{\Phi}{\Phi_0}\Big)\cos\varphi} \tag{15}$$

where $\epsilon = \frac{\hbar v_F}{R}$. The energy spectrum in Eq. (15) of the α-T_3 ring comprises a zero-energy flat band, along with a set of discrete levels in both the conduction and valence bands.

III. FORMALISM FOR THERMODYNAMIC QUANTITIES

In this section, we will calculate the thermodynamic properties of a monolayer α-T_3 QR, which is in contact with a thermal reservoir at a finite temperature. These properties encompass fundamental thermodynamic quantities, specifically the Helmholtz free energy, the internal energy, entropy, and heat capacity. We will exclusively focus on stationary states characterized by positive energy ($E > 0$) to constitute the thermodynamic ensemble. Given the strict exclusion of particle-particle interactions, the excitation of negative-energy states and the issue of pair production do not come into play [27, 28]. Consequently, the partition function involves a summation solely over positive-energy states, simplifying the analysis considerably. We commence by assessing the corresponding partition function as,

$$Z = \sum_{m=0}^{\infty} e^{-\beta E_2^+} \tag{16}$$

where $\beta = \frac{1}{k_B T}$, k_B is the Boltzmann constant and T is the equilibrium temperature. Rearranging the expressions in Eq. (15) and using Eq. (16), we obtain that for a one-fermion confined in the α-T_3 QR the partition function is,

$$Z = \sum_{m=0}^{\infty} e^{-\beta\sqrt{\mathcal{A}m^2+\mathcal{B}m+\mathcal{C}}} \tag{17}$$

where the quantities are,

$$\begin{aligned} \mathcal{A} &= \epsilon^2 \\ \mathcal{B} &= \epsilon^2\Big(2\frac{\Phi}{\Phi_0} - \cos 2\varphi\Big) \\ \mathcal{C} &= \epsilon^2\Big(\frac{1}{4} + \frac{\Phi^2}{\Phi_0^2} - \xi\frac{\Phi}{\Phi_0}\cos 2\varphi\Big). \end{aligned} \tag{18}$$

Since Eq. (17) cannot be evaluated analytically in a closed form, we consider the limit of a strong magnetic field ($\Phi \gg \Phi_0$). In this regime, the expression inside the summation can be approximated by $e^{-\beta\sqrt{\mathcal{B}m+\mathcal{C}}}$, which is a monotonously decreasing function. This allows us to approximate the summation by an integral, facilitating analytical progress in evaluating the partition function Z and further, the associated integral is,

$$\int_0^{\infty} e^{-\beta\sqrt{\mathcal{B}x+\mathcal{C}}}dx = \frac{2}{\mathcal{B}\beta^2}(1+\beta\sqrt{\mathcal{C}})e^{-\beta\sqrt{\mathcal{C}}}. \tag{19}$$

This integral is finite, and by the integral test, it guarantees the convergence of the original series. To evaluate the partition function in Eq. (17) in the high-field limit, we employ the Euler–Maclaurin summation formula, which provides a systematic way to approximate a discrete sum by an integral plus correction terms. The formula is given by [22, 29],

$$\sum_{n=0}^{\infty} f(n) = \frac{f(0)}{2} + \int_0^{\infty} f(x)dx - \sum_{p=1}^{\infty}\frac{B_{2P}f^{(2p-1)}(0)}{(2p)!}, \tag{20}$$

which may be rewritten simply as,

$$\sum_{n=0}^{\infty} f(n) \simeq \frac{f(0)}{2} + \int_0^{\infty} f(x)dx - \frac{f'(0)}{12} + \frac{f'''(0)}{720} - ..., \tag{21}$$

where B_{2p} is the Bernoulli number. Using the above equation we can rewrite the partition function Eq. (17) exactly as,

$$Z \simeq e^{-\beta\sqrt{\mathcal{C}}}\Big[\frac{2}{\mathcal{B}\beta^2}\Big(1+\beta\sqrt{\mathcal{C}}\Big) + \frac{1}{2} + \Big(\frac{\mathcal{B}}{24\sqrt{\mathcal{C}}} - \frac{\mathcal{B}^3}{720\sqrt{\mathcal{C}^5}}\Big)\beta + \frac{1}{90}\Big(\frac{\mathcal{A}}{2\mathcal{C}} - \frac{\mathcal{B}^2}{8\mathcal{C}^2}\Big)\beta^2 - \mathcal{O}(\beta^3)\Big] \tag{22}$$

where $f(n) = e^{-\beta\sqrt{\mathcal{B}n+\mathcal{C}}}$ and $\mathcal{O}(\beta^3)$ denotes higher-order terms in β, which will be neglected in the following analysis. In the high-temperature regime ($\beta \ll 1$), Eq. (22) becomes,

$$Z \simeq \frac{2}{\mathcal{B}\beta^2}\Big(1+\beta\sqrt{\mathcal{C}}\Big). \tag{23}$$

Given the thermal stability of graphene at high temperatures [30], we extend our analysis to investigate the thermodynamic properties of the α-T_3 quantum ring. Specifically, for a system of N non-interacting fermions the total partition function Z_N can be approximated by,

$$Z_N \simeq \left[\frac{2}{\mathcal{B}\beta^2}\Big(1+\beta\sqrt{\mathcal{C}}\Big)\right]^N. \tag{24}$$

Therefore, using the partition function given in Eq. (24), we can determine all associated thermodynamic quantities. After some algebraic manipulation, the Helmholtz free energy F, internal energy U, entropy S, and heat capacity C_V are obtained as follows,

$$F = -\frac{1}{\beta}\ln Z_N = -\frac{N}{\beta}\ln\left[\frac{2}{\mathcal{B}\beta^2}\Big(1+\beta\sqrt{\mathcal{C}}\Big)\right], \tag{25}$$

$$U = -\frac{\partial}{\partial\beta}\ln Z_N = N\frac{2+\beta\sqrt{\mathcal{C}}}{\beta(1+\beta\sqrt{\mathcal{C}})}, \tag{26}$$

$$S = k_B\beta^2\frac{\partial F}{\partial\beta} = Nk_B\left[\ln\Big\{\frac{2\Big(1+\beta\sqrt{\mathcal{C}}\Big)}{\mathcal{B}\beta^2}\Big\} + \frac{\Big(2+\beta\sqrt{\mathcal{C}}\Big)}{\Big(1+\beta\sqrt{\mathcal{C}}\Big)}\right], \tag{27}$$

$$C_V = -k_B\beta^2\frac{\partial U}{\partial\beta} = Nk_B\frac{2+4\beta\sqrt{\mathcal{C}}+\beta^2\mathcal{C}}{(1+\beta\sqrt{\mathcal{C}})^2}. \tag{28}$$

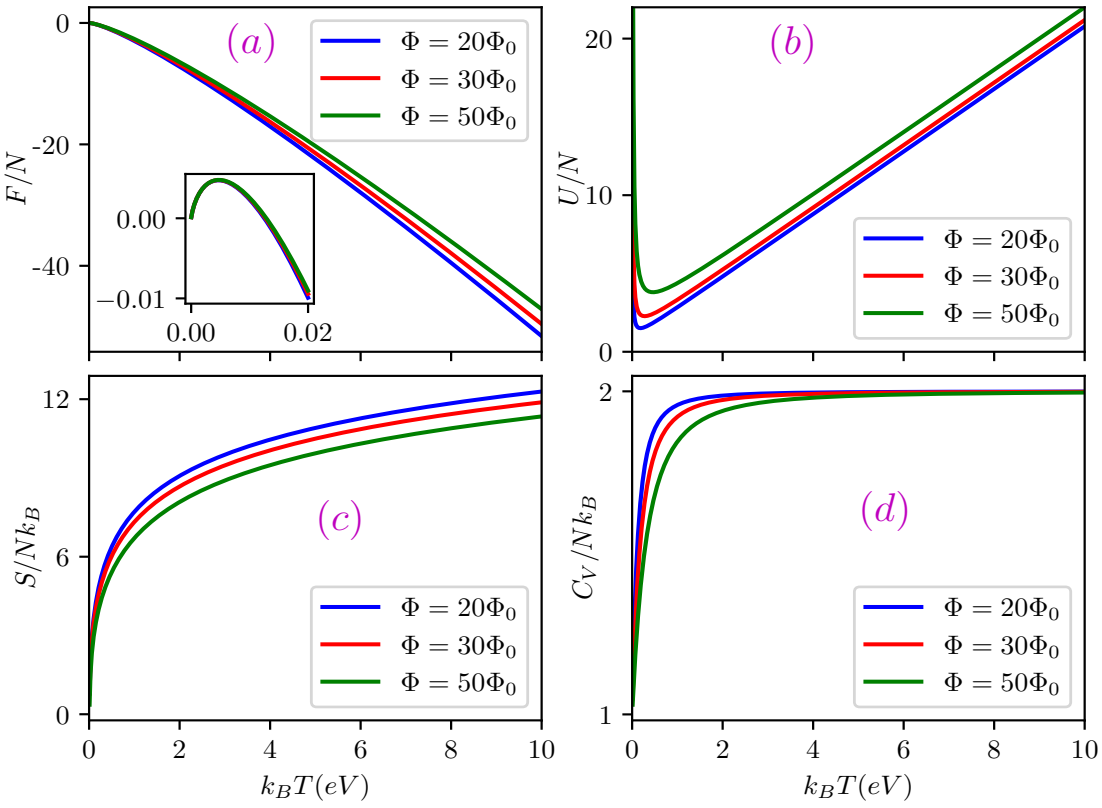

FIG. 2. (Color online) Thermodynamic properties (a) Helmholtz free energy, (b) internal energy, (c) entropy, and (d) heat capacity of the α-T_3 QR are displayed as function of temperature k_BT, with varying values of $\Phi = 20\Phi_0, 30\Phi_0$, and $50\Phi_0$. These results are obtained for a fixed α, namely, $\alpha = 0.5$. The ring radius is set to $R = 10$ nm.

IV. RESULTS AND DISCUSSIONS

We applied the Euler-Maclaurin formula, especially tailored for a strong magnetic field, to compute the partition function. It is worth noting that our theory involves two key parameters of interest, the coupling parameter, α, and the external magnetic flux, Φ. In Fig. 2 we investigate all the profiles of the thermal quantites given in Eqs. (25)-(28) as a function of temperature k_BT by varying magnetic flux values: $\Phi = 20\Phi_0, 30\Phi_0$, and $50\Phi_0$, while keeping $\alpha = 0.5$ constant. In Fig. 2(a), we can observe that the Helmholtz function, $\frac{F}{N}$, experiences a marginal increase as k_BT starts to rise at very low temperatures, as depicted in the inset figure. However, after reaching its peak, it exhibits nearly linear decline as k_BT continues to increase, while changing with the varying Φ.

Figure 2(b) reveals that for low temperatures in the range of $0 < k_BT < k_BT_c$, the behavior of the internal energy, $\frac{U}{N}$, decreases with the increasing temperature regardless of the magnetic flux values. However, beyond the critical temperature, it begins to increase in an almost linear fashion, with a more pronounced

growth as Φ increases.

The entropy, $\frac{S}{Nk_B}$, remains unaffected by the external flux within the temperature range of $0 < k_BT < k_BT_c$. Nevertheless, beyond this temperature threshold, $\frac{S}{Nk_B}$ exhibits slight variations in relation to Φ. Notably, for larger values of Φ, $\frac{S}{Nk_B}$ decreases, as shown in Fig. 2(c).

Moreover, in Fig. 2(d), we can observe that the heat capacity, $\frac{C}{Nk_B}$, converges to a fixed value of 2 as k_BT increases, regardless of the magnetic flux, displaying an asymptotic behaviour.

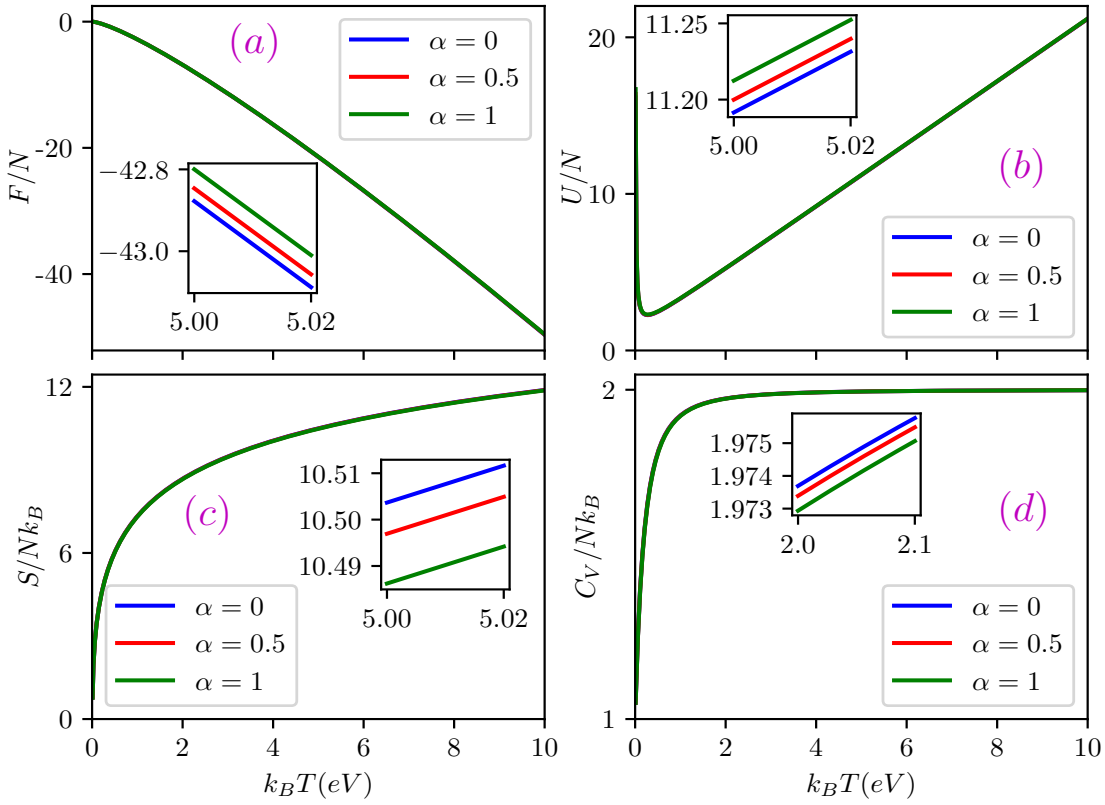

FIG. 3. (Color online) Thermodynamic properties of the α-T_3 QR are displayed as function of temperature k_BT, with varying values of $\alpha = 0, 0.5$, and 1. These results are obtained for a fixed magnetic flux $\Phi = 30\Phi_0$. (a) the Helmholtz free energy, (b) the internal energy, (c) the entropy, and (d) the heat capacity. The ring radius is set to $R = 10$ nm.

From Fig. 3(a) we explore the second case with varying α values, where we observe that the Helmholtz function $\frac{F}{N}$ decreases with an approximately linear behaviour when k_BT increases and it has higher values when α increases, although the dependency on α is negligible. In Fig. 3(b) for the very low temperature we observe that the internal energy $\frac{U}{N}$ decreases with temperature, after attaining minima it increases nearly linearly with k_BT. However, the nature slightly depends on the values of α. As α decreases, the curve of the internal energy grows faster. The entropy $\frac{S}{Nk_B}$ is almost independent while showing a small variation in terms of α, as decreases for large α's as depicted in the inset of Fig. 3(c). The heat capacity, $\frac{C}{Nk_B}$, tends

to an asymptotic behaviour, converging to a fixed value of 2 as k_BT increases which is shown in Fig. 3(d).

By analysing the nature of the curves representing our focused thermodynamic functions, we can gain insights into the thermal behaviour of our system. We observe that the Helmholtz free energy, in both cases, exhibits a critical point at low temperatures, specifically in proximity to $T = 0$. As the system's temperature increases, the available free energy for performing ensemble work rapidly diminishes. Conversely, when this ensemble moves toward thermal equilibrium within the reservoir, the system's internal energy steadily increases. Additionally, the thermal variations of the α-T_3 QR tend to rise until it reaches thermal equilibrium in both scenarios. Once equilibrium is achieved, the heat capacity remains unchanged. Moreover, in accordance with principles from solid-state physics, we can observe that our system satisfies the well-known Dulong-Petit law. This law is characterized by $\frac{C_V}{N} \simeq 2k_B$, as evident in both Figs. 2(d) and 3(d). Furthermore, the qualitative features of the thermodynamic functions remain consistent across all values of α.

V. SUMMARY AND CONCLUSIONS

In summary, we conducted a comprehensive investigation into the thermodynamic characteristics of the α-T_3 quantum ring within a heat bath, following the canonical ensemble at finite temperature. Our key findings are as follows.

Due to the absence of a closed-form expression for the exact partition function, we adopted the strong field approximation and applied the Euler–Maclaurin summation formula for numerical evaluation. Once the partition function was determined, it paved the way for deriving all the key thermodynamic quantities, including the Helmholtz free energy F, internal energy U, entropy S, and heat capacity C_V. We generated graphical representations of these quantities for various λ_R values and distinct magnetic fluxes Φ. The outcomes of our study highlighted the satisfaction of the well-established Dulong-Petit law. We anticipate that our findings will serve as a valuable tool for examining these thermal properties in connection with experimental investigations.

In conclusion, by tuning the parameters α and Φ, the thermodynamic properties of the system can be effectively controlled, making them tunable features that reflect the interplay between lattice geometry and magnetic flux.

* mislam@iitg.ac.in

[1] V. M. Fomin (Editor), *Physics of Quantum Rings, in NanoScience and Technology*, (Springer-Verlag, Berlin, Heidelberg, 2014).

[2] T. Nowozin, *Self-organized Quantum Dots for Memories: Electronic Properties and Carrier Dynamics*, Springer Theses (Springer, 2014).

[3] P. Michler, *Single Quantum Dots: Fundamentals, Applications, and New Concepts*, Vol. 90 (Springer-Verlag, Berlin, 2003).

[4] M. I. Katsnelson, Graphene: Carbon in Two Dimensions (Cambridge University Press, Cambridge, 2012).

[5] B. Sutherland, Phys. Rev. B **34**, 5208 (1986).

[6] J. Vidal, R. Mosseri, and B. Doucot, Phys. Rev. Lett. **81**, 5888(1998).

[7] F. Wang and Y. Ran, Phys. Rev. B **84**, 241103(R) (2011).

[8] D. F. Urban, D. Bercioux, M. Wimmer, and W. Husler, Phys. Rev. B **84**, 115136 (2011).

[9] J. D. Malcolm and E. J. Nicol, Phys. Rev. B **92**, 035118 (2015).

[10] E. Illes, J. P. Carbotte, and E. J. Nicol, Phys. Rev. B **92**, 245410 (2015).

[11] T. Biswas and T. K. Ghosh, J. Phys.: Condens. Matter **28**, 495302 (2016).

[12] E. Illes and E. J. Nicol, Phys. Rev. B **94**, 125435 (2016).

[13] A. D. Kovacs, G. David, B. Dora, and J. Cserti, Phys. Rev. B **95**, 035414 (2017).

[14] D. O. Oriekhov and V. P. Gusynin, Phys. Rev. B **101**, 235162 (2020).

[15] J. Wang, J. F. Liu, and C. S. Ting, Phys. Rev. B **101**, 205420 (2020).

[16] B. Dey, P. Kapri, O. Pal, and T. K. Ghosh, Phys. Rev. B **101**, 235406 (2020).

[17] J. Wang and J. F. Liu, Phys. Rev. B **103**, 075419 (2021).

[18] R. Soni, N. Kaushal, S. Okamoto, and E. Dagotto, Phys. Rev. B **102**, 045105 (2020).

[19] A. A. Balandin, Nat. Mater. **10**, 569 (2011).

[20] A. Alofi and G.P. Srivastava, Phys. Rev. B **87**, 115421 (2013).

[21] J. Che, T. Cagin, and W.A. Goddard, Nanotechnology **11**, 65 (2000).

[22] R. R. S. Oliveira, A. A. A. Filho, F. C. E. Lima, R. V. Maluf, and C. A. S. Almeida, Eur. Phys. J. Plus **134**, 495 (2019).

[23] R. Houca and A. Jellal, Phys. Scr. **94**, 105707 (2019).

[24] N. Bolivar, E. Medina, and B. Berche, Phys. Rev. B **89**, 125413 (2014).

[25] D. R. da Costa, A. Chaves, M. Zarenia, J. M. Pereira Jr., G. A. Farias, and F. M. Peeters, Phys. Rev. B **89,** 075418 (2014).

[26] M. Islam, T. Biswas, and S. Basu, Phys. Rev. B **108**, 085423 (2023).

[27] Grandy Jr, Walter T. *Foundations of statistical mechanics: Equilibrium theory*. Vol. 19. Springer Science & Business Media, (2012).

[28] R. Houça and A. Jellal, Phys. Scr. **94**, 105707 (2019).

[29] W. Greiner, Ludwig Neise, Horst Stocker, D. Rischke, *Thermodynamics and Statistical Mechanics*, (Springer, New York, 1995).

[30] K. Kim, W. Regan, B. Geng, B. Alemán, B. M. Kessler, F. Wang, M. F. Crommie, and A. Zettl, Phys. Stat. Sol.

(RRL) **4**, 302 (2010).